Solid State Communications 151 (2011) 933–937

Contents lists available at ScienceDirect

Solid State Communications

journal homepage: www.elsevier.com/locate/ssc

Spin-glass and spin-fluctuation in Mo-doped $Ca_3Co_4O_9$ system

Yankun Fu [a,b], Bangchuan Zhao [b,*], Yanan Huang [b], Jie Yang [b], Jianming Dai [b], Mingdong Zhou [a], Yuping Sun [b]

[a] College of Science, Shandong University of Science and Technology, Qingdao 266510, People's Republic of China

[b] Key Laboratory of Materials Physics, Institute of Solid State Physics, and Hefei High Magnetic Field Laboratory, Chinese Academy of Sciences, Hefei 230031, People's Republic of China

ARTICLE INFO

Article history:
Received 31 January 2011
Received in revised form
3 April 2011
Accepted 11 April 2011
by P. Sheng
Available online 19 April 2011

Keywords:
A. Cobaltite
D. Spin-glass
D. Spin-fluctuation

ABSTRACT

Structural, magnetic, resistivity and thermal transport measurements have been performed to study the Mo-doping effect on a layered cobaltite $Ca_3Co_{4-x}Mo_xO_9$ ($0 \leq x \leq 0.4$) system. The results indicate that the low-temperature magnetic behavior of the system changes from a ferrimagnetic state to a spin-glass-like state upon Mo doping, which is due to the decrease in the average valence of Co ions. Moreover, all the Mo-doped samples have a higher resistivity and larger thermopower S compared with the Mo-free sample. The variation in the resistivity and thermopower between the Mo-doped and the Mo-free samples is dominated by the change in the carrier concentration of the samples. In the Mo-doped samples with $x \geq 0.1$, both the resistivity and thermopower decrease gradually with increasing Mo-doping level, which is suggested to mainly originate from the variation in the carrier mobility of the samples. In addition, an obvious thermopower upturn is observed in the $S(T)$ curve of all the Mo-doped samples, which can be explained by the enhancement of spin-fluctuation induced by Mo-doping.

1. Introduction

Since the discovery of high-temperature superconductivity in layered copper oxides, other layered 3d transition-metal oxides have also been extensively studied [1–5]. This has shown that there exists strong coupling among the degrees of freedom for the charge, spin, orbital, and lattice, which are essential for the emergence of complex physical phenomena such as giant magnetoresistance (GMR), superconductivity and thermoelectric effects [6–8]. Among these oxides, layered cobaltite Na_xCoO_2 and $Ca_3Co_4O_9$ have attracted considerable attention due to their unusual thermoelectric properties, i.e., larger room-temperature thermopower coexisting with the metallic-like electric conductivity and much lower thermal conductivity, which are beneficial to their potential thermoelectric applications [7,9]. Compared with Na_xCoO_2, the $Ca_3Co_4O_9$ system is considered to be a more suitable thermoelectric material due to its high-temperature stabilization even in an oxidizing atmosphere.

$Ca_3Co_4O_9$ is a misfit oxide and can be denoted as $[Ca_2CoO_3][CoO_2]_{b1/b2}$ to recognize the incommensurate nature of the structure. The structure is composed of alternating stacks along the c-axis of the CaO–CoO–CaO rock-salt-like layer (RS layer) and a CoO_2 cadmium iodide-like layer. The two layers have identical a, c and β but different b parameters [10]. The ratio of b_1 and b_2 is 1.62 [11], where b_1 refers to the b-axis length of the RS layer and b_2 denotes the b-axis length of the $[CoO_2]$ sub-lattice, so the mean Co–O band distance in the $[CoO_2]$ subsystem is shorter than that in the RS subsystem. The complicated structure induces rather complex physical properties in the system. For example, two magnetic transitions were observed around 19 K and 380 K corresponding to the ferrimagnetic and spin-state transitions, respectively [12–14]. Moreover, a short-range incommensurate spin-density-wave (IC-SDW) starts to occur below about 100 K and completes below about 30 K as evidenced in the $\rho(T)$ curve of the sample. With increasing temperature, the sample changes its transport behavior from a low-temperature insulator to a strongly correlated Fermi liquid, then to an incoherent metal, finally to a semiconductor at elevated temperature. The formation of IC-SDW is considered to be responsible for the metal–insulator transition near 80 K [13,14]. Moreover, the charge-carrier transport in the $Ca_3Co_4O_9$ system is mainly restricted to the CoO_2 layers and the carriers can be varied in a considerably wide range by element doping. Therefore, the substitution of some ions on Ca or Co sites to adjust the charge-carrier concentration, and then the thermopower and resistivity is a useful way to improve the thermal properties of the materials [15–22]. In general, doping on Ca-sites only changes the carrier concentration of the system and has less influence on the band structure. In contrast, doping on Co-sites, especially in the CoO_2 layer, can cause a large change in physical properties because the band structure and transport mechanism are affected [23,24].

* Corresponding author. Tel.: +86 551 559 1439; fax: +86 551 559 1434.
E-mail address: bchzhao@issp.ac.cn (B.C. Zhao).

0038-1098/$ – see front matter
doi:10.1016/j.ssc.2011.04.009

In order to further understand the unusual properties of $Ca_3Co_4O_9$ system, we carefully investigate the effect of Mo-doping at Co-sites on the structural, magnetic, electrical transport and thermoelectric characteristics in cobaltite $Ca_3Co_{4-x}Mo_xO_9$ ($0 \leq x \leq 0.4$) ceramics. We found that the Mo ions can have a strong effect on the magnetic, electrical and thermal transport properties of the system, and the thermopower of the $Ca_3Co_4O_9$ system can be improved by the substitution of Mo for Co ions.

2. Experimental details

A series of polycrystalline samples of $Ca_3Co_{4-x}Mo_xO_9$ ($x = 0, 0.1, 0.2, 0.3$, and 0.4) were prepared by a sol–gel method. Stoichiometric amounts of high-purity $CaCO_3$ powders were dissolved in diluted nitric acid, followed by the addition of stoichiometric amounts of $Co(NO_3)_2.6H_2O$ and $(NH_4)_6Mo_7O_{24} \cdot 4H_2O$ dissolved in distilled water with continuous stirring, and then citric acid was added to make a solution complex. After all the reactants had been completely dissolved, the solution was heated on a hot plate resulting in the formation of a gel. The gel was dried at 300 °C, and then preheated to 650 °C to remove the remaining organics and decompose the nitrates of the gel. The obtained powders were ground, pelletized, and sintered at 900 °C for 10 h in air. Then the black ceramic pellets of $Ca_3Co_{4-x}Mo_xO_9$ were obtained.

The structure and phase purity of the samples were examined by the powder X-ray diffraction (XRD) using a Philips X'Pert PRO X-ray diffractometer with CuK_α radiation at room temperature. The microstructure was identified by field-emission scanning electron microscopy (SEM) equipment. The magnetic properties of the studied samples were measured with a superconducting quantum interference device (SQUID) measurement system. The resistivity and thermal transport properties were determined using the standard four-probe method in a commercial Physical Property Measurement System (PPMS) in the temperature range of 5–320 K.

3. Results and discussion

Fig. 1 shows the powder XRD patterns for the $Ca_3Co_{4-x}Mo_xO_9$ ($x = 0, 0.1, 0.2, 0.3$, and 0.4) samples at room temperature. The XRD patterns of all studied samples are identical to the standard JCPDS card and the reported data for the $Ca_3Co_4O_9$ structure [9], indicating the formation of single-phase compounds. The result shows that the Mo-doping does not change the structure of the system and all the diffraction peaks shown in the main panel of Fig. 1 can be well indexed with a monoclinic lattice. It should be noted that the XRD profiles of the samples exhibit much stronger diffraction peaks from the (00l) planes, indicating the formation of textured structures in these polycrystalline samples. The micrographs perpendicular and parallel to the pressing axis for the $x = 0$ sample are shown in Fig. 2. The results reveal that the sample is textured and exhibits a quasi2-dimension layered structure. In order to display the effect of Mo-doping on the $Ca_3Co_4O_9$ lattice, the enlarged (003) diffraction peaks of the studied samples are shown in the inset of Fig. 1. It can be seen clearly that the diffraction peaks shift to a lower angle with the increase in the Mo-doping level. The result is consistent with the fact that the ionic radius of Mo^{6+} ions (0.59) is larger than that of Co^{3+} in a low spin-state (0.545) and Co^{4+} (0.53) ions using the coordination number six [14,25].

The temperature dependence of dc magnetization M of $Ca_3Co_{4-x}Mo_xO_9$ ($0 \leq x \leq 0.4$) samples under the zero-field-cooled (ZFC) mode at an applied magnetic field of 0.1 T is shown in the main panel of Fig. 3. The measurements were performed in a wide temperature range of 5–320 K and only the

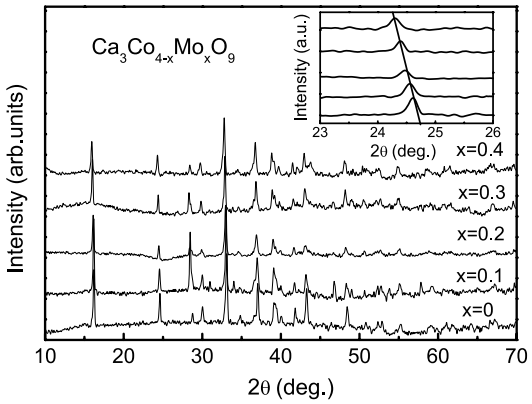

Fig. 1. XRD patterns of $Ca_3Co_{4-x}Mo_xO_9$ ceramics ($0 \leq x \leq 0.4$). The inset shows the shift of the (003) peaks due to variation of the Mo doping content.

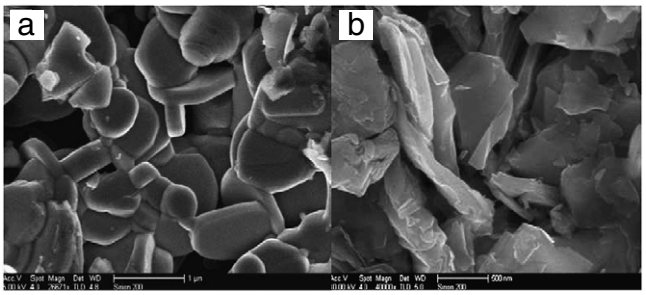

Fig. 2. SEM micrographs of the $Ca_3Co_4O_9$ sample perpendicular (a) and parallel (b) to the pressing axis, respectively.

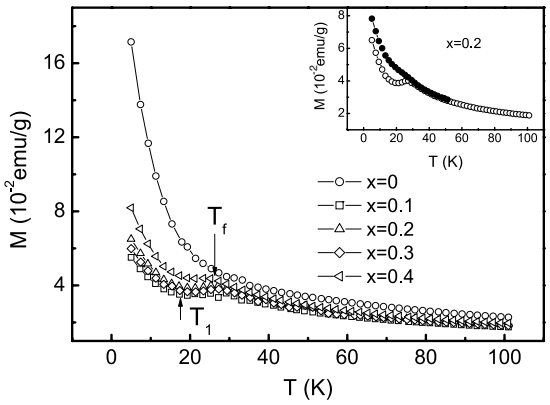

Fig. 3. Temperature dependence of ZFC magnetization M for all samples. The inset shows the ZFC and FC magnetization curves for the sample with $x = 0.2$.

data in the low-temperature range below 100 K are shown in the figure. The Mo-free sample $Ca_3Co_4O_9$ shows a similar magnetic behavior with the data reported earlier in the literature [14]: a paramagnetic behavior in the high temperature range above 50 K and a ferrimagnetic-like transition at about 19 K. However, the magnetization curves of the Mo-doped samples are more complicated compared with that of the Mo-free sample. The high-temperature (above 50 K) paramagnetic behavior persists when partial Co ions in the system are substituted by Mo. As temperature decreases, an obvious cusp at T_f (defined as the freezing temperature) and a valley at T_1 in the ZFC $M(T)$ curve for the Mo-doped samples are observed. The temperature dependence of magnetization $M(T)$ was also measured under field-cooled (FC) mode at 0.1 T field. The FC $M(T)$ curve almost overlaps with the ZFC one for the undoped sample $Ca_3Co_4O_9$, whereas it deviates from the ZFC curve significantly for the Mo-doped samples. A typical FC result of the Mo-doped sample with $x = 0.2$ along

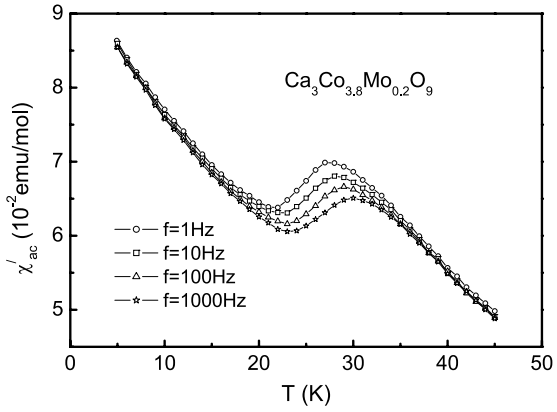

Fig. 4. AC susceptibility vs temperature for the sample with Mo-doping level $x = 0.2$.

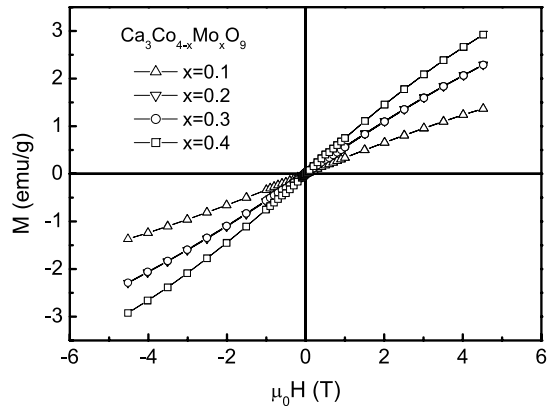

Fig. 5. Field dependence of magnetization for the Mo-doped samples at 5 K.

with its ZFC data is plotted in the inset of Fig. 3 as an example. A similar M (T) result was also observed in the high-valence Ti ion doped $Ca_3Co_4O_9$ system [15]. Therefore, it is suggested that the observed phenomenon maybe a universal result for high-valence ion doping at Co-sites in the $Ca_3Co_4O_9$ system. In general, the distinctive separation between the FC and ZFC $M(T)$ curves at low temperatures can be ascribed to the appearance of the spin-glass or cluster-glass state induced by the competition between the FM and antiferromagnetic (AFM) interactions. The glass state induced by Mo-doping can be further proved by the temperature dependence of ac susceptibility χ'_{ac} as shown in Fig. 4, where the susceptibility becomes frequency dependent in the temperature range of T_f and T_1.

From Fig. 3, we can see that all Mo-doped samples show a lower value of magnetization compared with the undoped sample and the $x = 0.1$ sample has the lowest magnetization in the series of samples. That is to say, as the Mo-doping level exceeds a certain value, such as $x = 0.1$, the magnetization increases with increasing Mo-doping content. The variation trend can be further confirmed by the field dependent magnetization curve as shown in Fig. 5. In order to clarify, the values of the magnetization at T_f (M_f) and 300 K $(M_{300\,K})$ along with T_f and T_1 are listed in Table 1. This shows that the T_f peak position shifts to a lower temperature and the T_1 position shifts to a higher temperature with increasing Mo-doping content. As we know, there exist complex magnetic interactions in the $Ca_3Co_4O_9$ system. The ferrimagnetism in the system is mainly caused by the interlayer coupling between CoO_2 and Ca_2CoO_3 subsystems. In addition, superexchange (SE) and double exchange (DE) interactions between Co^{3+} and Co^{4+} ions are considered to coexist in the system. Based on the valence equilibrium, Mo doping into $Ca_3Co_4O_9$ system will transfer partial Co^{4+} ions into Co^{3+} or

Table 1
Magnetic and electrical transport properties of $Ca_3Co_{4-x}Mo_xO_9$ $(0 \le x \le 0.4)$ ceramics.

	$x = 0$	$x = 0.1$	$x = 0.2$	$x = 0.3$	$x = 0.4$
T_f (K)	...	28.6	27.7	26.8	25.4
T_1 (K)	...	18.5	19.0	19.7	21.1
M_f (emu/g)	...	3.59	3.81	4.01	4.38
$M_{5\,K}$(emu/g)	17.15	5.51	5.99	6.50	8.19
T_{min} (K)	78.9	146.9	155.3	156.1	180.8
$\rho_{300\,K}$ (Ωcm)	0.023	0.0534	0.0511	0.0394	0.0346
ρ_{Tmin} (Ωcm)	0.0132	0.0504	0.0464	0.0366	0.0317
T_0 (K^3)	270.6	4.71×10^3	4.23×10^3	4.01×10^3	0.68×10^3

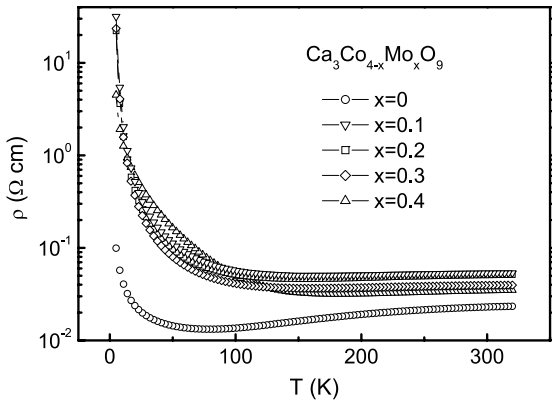

Fig. 6. Resistivity as a function of temperature under zero magnetic field for the studied samples.

Co^{2+}, which will destroy the interlayer coupling between different subsystems resulting in the abrupt decrease of magnetization. With further increasing Mo-doping content, the DE interaction enhances and competes with the SE interaction giving rise to the appearance of the SG state, and the magnetization increases.

Fig. 6 shows the electrical resistivity as a function of temperature for $Ca_3Co_{4-x}Mo_xO_9$ (x = 0, 0.1, 0.2, 0.3 and 0.4) samples at zero magnetic field. The following features are noted: (1) The electrical resistivity $\rho(T)$ shows a metallic-like temperature dependent behavior down to a certain temperature T_{min} and a metal–insulator (M–I) transition occurs in the low-temperature region for all studied samples. The temperature dependence of resistivity behavior is quite similar to the in-plane resistivity $\rho_{ab}(T)$ of a single crystal as reported earlier [26], implying the electrical transport behavior in the present samples is governed by ρ_{ab}. (2) The transition temperature T_{min} shifts to a higher temperature as the Mo-doping content increases and the value of the transition temperature is shown in Table 1. The M–I transition in the $Ca_3Co_4O_9$ system is always considered to be related to the localization of charger carriers caused by the IC-SDW and the transition strongly depends on the average valence of Co ions in the samples [12–14,20]. So, the increase in T_{min} in the present samples may be related to the decrease in the average valence of Co ions due to the high-valence Mo^{6+}-doping. (3) All $\rho(T)$ curves of the Mo-doped samples exhibit higher resistivity ρ compared with the $Ca_3Co_4O_9$ specimen. In the $Ca_3Co_4O_9$ system, the main carriers are holes. On the basis of valence equilibrium, the substitution of Mo^{6+} for Co ions will decrease the average valence of Co ions and then decrease the holes in the system. The increase of ρ in Mo-doped samples should be attributed to the decrease of holes as aforementioned. (4) As the Mo-doping level increases further from $x = 0.1$, the resistivity decreases slowly. That is to say, the sample with $x = 0.1$ has the largest resistivity in the series of samples, which may be related to the increase in the carrier mobility due to Mo-doping in the samples comparable with the case in the Bi-doped $Ca_2Co_2O_5$ system [27]. In general, the variation in the resistivity for a doped

specimen is always determined by the change in the concentration or mobility of the carriers. For the sample with $x \leqslant 0.1$, Mo substitution mainly occurs in the CoO_2 layers and induces a sudden decrease in holes n giving rise to the increase in the resistivity compared with the undoped sample. As $x > 0.1$, Mo ions will mainly enter into the Ca_2CoO_3 layers and the carrier concentration n in the system decreases slowly and its influence on the resistivity is minor. The average distance between carriers increases due to the decrease in n, resulting in the increase in the mobility of the carriers, and therefore the resistivity of the Mo-doped samples decreases with increasing Mo-doping content from $x = 0.1$. This supposition can be further proved by the thermal measurement as discussed below. It should be noted that the obtained result is contrary to the electron-doping effect at Ca-sites in the $Ca_3Co_4O_9$ system [20].

To explore the reason for the variations in the transport properties induced by Mo-doping, next we investigate the transport mechanism of the studied samples. Firstly, we focus on the transport mechanism of the low-temperature SDW state for the studied samples. Normally, the variation in the resistivity with temperature for the $Ca_3Co_4O_9$ system follows the expression:

$$\frac{1}{\rho} = \mu(T) \exp\left(-\frac{E_0}{k_B T}\right), \tag{1}$$

where $\mu(T)$ is the mobility of carriers and E_0 is the energy gap resulting from the SDW state at the Fermi surface [14,19]. However, we find that only the $\rho(T)$ curve for the undoped sample can be well fitted using Eq. (1). As for the Mo-doped samples, Mott's two-dimensional variable range hopping (2D-VRH) model can describe the experimental data well. That is to say, the Mo-doping level of 0.1 at the Co-site in $Ca_3Co_4O_9$ is sufficient to change the transport mechanism from thermally activated behavior to the 2D-VRH one. The suddenly decrease in the carrier concentration n may be the origin of the variation in the transport mechanism upon Mo-doping. According to the VRH theory, the relation between resistivity and temperature in a 2D system can be expressed as:

$$\rho(T) = \rho(0) \exp\left(\frac{T_0}{T}\right)^{1/3}, \tag{2}$$

where $\rho(0)$ is a constant, T_0 is the VRH characteristic temperature associated with the localization length l_v and the density of states $N(\varepsilon_F)$ in the vicinity of the Fermi energy level, i.e., $k_B T_0 = 8/[\pi N(\varepsilon_F) l_v^2]$. Fig. 7 shows the fit curves for the undoped (inset) and the Mo-doped samples (main panel) based on Eqs. (1) and (2), respectively. The obtained fit parameters T_0 are listed in Table 1. It is found that the T_0 value decreases obviously with the increase in the Mo-doping content, implying the increase in the localization length and enhancement of the carrier mobility. The result is contrary to that observed in the electron-doping at Ca-sites in the $Ca_3Co_4O_9$ system. Similar results can also be found in Mo-doped single crystals prepared by the flux-growth method [28]. The detailed reason of this phenomenon is under study.

To test the thermoelectric properties, the temperature dependence of thermopower S of the samples at zero magnetic field is measured and the result is shown in Fig. 8. All the samples exhibit positive values of thermopower over the entire temperature range, indicating p-type materials and positive hole conduction dominating the transport properties. For the Mo-free sample $Ca_3Co_4O_9$, Fig. 8 shows that S decreases slowly with decreasing temperature down to about 10 K with a small variation in the slope of the curve near 130 K. As the temperature decreases further from 10 K, S decreases rapidly. The result is in accordance with the in-plane thermopower behavior of a single-crystal with the same composition reported earlier [29]. The Mo-doped samples do not change the high-temperature positive temperature dependence of the S (T) behavior significantly. However, in the low-temperature range

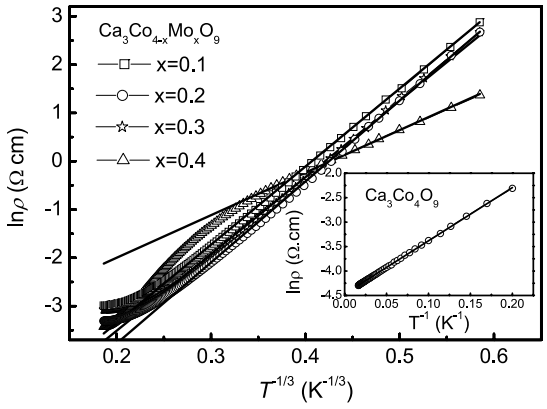

Fig. 7. The fitting plot of $\rho(T)$ curves to the 2D-VRH model at low-temperatures for the Mo-doped samples. The inset shows the fitting plot according to the TA model for the free-doped sample at low temperatures.

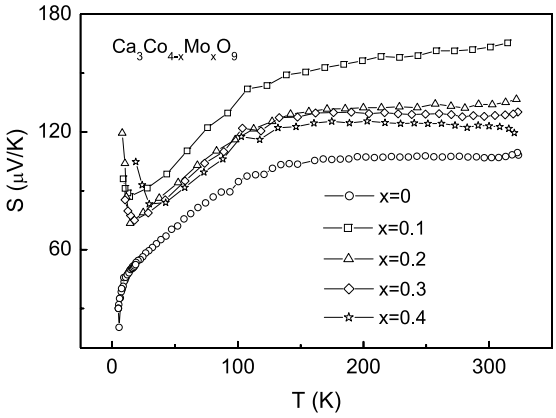

Fig. 8. Temperature dependence of thermopower at zero field for all studied samples.

below about 50 K, all the Mo-doped samples show a distinct minimum of the thermopower at $T_{S\min}$ which depends on the Mo-doping concentration. As the temperature decreases further, $S(T)$ shows a steeper upturn. A similar thermopower upturn at low temperatures is also observed in the Ti- or Lu-doped $Ca_3Co_4O_9$ system [19,22]. The S upturn is suggested to originate from the enhanced spin-fluctuation at low-temperatures due to Mo-doping. As the Mo^{6+} ions are doped into the $Ca_3Co_4O_9$ system, the distance between different layers will increase and the correlation between Co ions will be blocked and then the spin-fluctuation enhances. This hypothesis can be further testified by the comparison of the temperature dependence of thermopower behavior under 0 and 5 T applied field as shown in Fig. 9. The thermopower upturn is weakened due to the suppression of the spin-fluctuation by the applied magnetic field.

From Fig. 8, we can see that all the Mo-doped samples show a larger thermopower compared with the undoped sample and the $x = 0.1$ sample has the largest thermopower at all temperatures. That is to say, a small quantity of Mo doping into the $Ca_3Co_4O_9$ system can bring a sudden increase in thermopower, but S decreases as the Mo-doping content increases further from $x = 0.1$. The result is in agreement with resistivity properties for the studied samples as discussed above. The unusual change behavior can be explained by the collective effect of the variation in the carrier concentration and carrier mobility. In general, the thermopower of a layered correlated system can be expressed by the Mott formula [20]:

$$S(T) = \frac{\pi^2 k_B^2 T}{3e} \left[\frac{\partial \ln \sigma(\varepsilon)}{\partial \varepsilon}\right]_{\varepsilon=\varepsilon_F}, \tag{3}$$

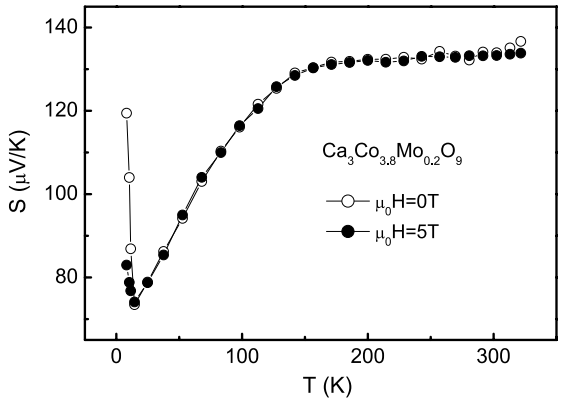

Fig. 9. Thermopower vs temperature at applied magnetic field of 0 and 5 T for the sample with $x = 0.2$.

where $\sigma(\varepsilon)$ and k_B are the electric conductivity at energy ε and Boltzmann constant. By substituting $\sigma = en\mu(\varepsilon)$ in the formula, Eq. (3) can turn into

$$S(T) = \frac{C_e}{n} + \frac{\pi^2 k_B^2 T}{3e}\left[\frac{\partial \ln \mu(\varepsilon)}{\partial \varepsilon}\right]_{\varepsilon=\varepsilon_F}, \quad (4)$$

where C_e, n, and μ (ε) are the electronic specific heat, carrier concentration, and energy correlated carrier mobility, respectively. As aforementioned, for the $x = 0.1$ sample, the Mo-doping mainly occurs in the CoO_2 layer and leads to a sudden decrease in the carrier concentration, so the thermopower of the system is mainly determined by the first term of Eq. (4). However, as the Mo-doping level is larger than 0.1, a larger amount of Mo ions will enter the Ca_2CoO_3 layers and the carrier concentration changes slowly. In this case, the thermal transport properties of the system are mostly dominated by the variation in the carrier mobility μ (ε) as described by the second part in Eq. (4). As discussed above, the carrier mobility of the Mo-doped samples increases with increasing Mo-doping content but its change rate decreases obviously. This is the reason why the thermopower decreases slowly with increasing Mo-doping content in the Mo-doped samples.

4. Conclusions

In summary, the Mo-doping effect on the structural, magnetic, electric and thermal transport properties of the $Ca_3Co_4O_9$ system have been studied systematically. The Mo-doping does not change the high-temperature PM behavior of the system, but leads to the magnetic transition from a low-temperature ferrimagnetic state to a spin-glass-like magnetic phase by the introduction of only 0.1 Mo-ions. The result may be related to the decrease in the average valence of Co ions in the material. There are few changes in the behavior of the temperature dependence of resistivity and thermopower except for the low-temperature thermopower upturn for the Mo-doped samples. However, the resistivity is much higher and the thermopower is much larger for the Mo-doped samples compared with the undoped sample. The variation in the resistivity and thermopower between the Mo-doped and Mo-free samples is dominated by the change in the carrier concentration, and the low-temperature thermopower upturn originates from the spin-fluctuation. In addition, both the resistivity and thermopower of the Mo-doped samples decrease with increasing the Mo-doping concentration, which is due to the increase in the carrier mobility and the decrease in the variation rate of the carrier mobility.

Acknowledgments

This work was supported by the Nature Science Foundation of Anhui Province of China under Contract No. 090414184 and the National Nature Science Foundation of China under Contract No. 10974205.

References

[1] C.H. Chen, S.W. Cheong, A.S. Cooper, Phys. Rev. Lett. 71 (1993) 2461.
[2] Y. Murakami, H. Kawada, H. Kawata, M. Tanaka, T. Arima, Y. Moritomo, Y. Tokura, Phys. Rev. Lett. 80 (1998) 1932.
[3] A.P. Mackenzie, Y. Maeno, Rev. Modern Phys. 75 (2003) 657.
[4] R. Funahashi, I. Matsubara, H. Ikuta, T. Takeuchi, U. Mizutani, S. Sodeoka, Jpn. J. Appl. Phys. Part 2-Lett. 39 (2000) L1127.
[5] Y.Y. Wang, N.S. Rogado, R.J. Cava, N.P. Ong, Nature 423 (2003) 425.
[6] M.N. Baibich, J.M. Broto, A. Fert, F.N. Van Dau, F. Petroff, P. Etienne, G. Creuzet, A. Friederich, J. Chazelas, Phys. Rev. Lett. 61 (1988) 2472.
[7] I. Terasaki, Y. Sasago, K. Uchinokura, Phys. Rev. B 56 (1997) R12685.
[8] S. Jin, T.H. Tiefel, M. McCormack, R.A. Fastnacht, R. Ramesh, L.H. Chen, Science 264 (1994) 413.
[9] A.C. Masset, C. Michel, A. Maignan, M. Hervieu, O. Toulemonde, F. Studer, B. Raveau, J. Hejtmanek, Phys. Rev. B 62 (2000) 166.
[10] S. Lambert, H. Leligny, D. Grebille, J. Solid State Chem. 160 (2001) 322.
[11] Y. Miyazaki, M. Onoda, T. Oku, M. Kikuchi, Y. Ishii, Y. Ono, Y. Morii, T. Kajitani, J. Phys. Soc. Jpn. 71 (2002) 491.
[12] J. Sugiyama, C.T. Xia, T. Tani, Phys. Rev. B 67 (2003) 104410.
[13] J. Sugiyama, H. Itahara, T. Tani, J.H. Brewer, E.J. Ansaldo, Phys. Rev. B 66 (2002) 134413.
[14] J. Sugiyama, J.H. Brewer, E.J. Ansaldo, H. Itahara, K. Dohmae, Y. Seno, C. Xia, T. Tani, Phys. Rev. B 68 (2003) 134423.
[15] B.C. Zhao, Y.P. Sun, Song W.H., J. Appl. Phys. 99 (2006) 073906.
[16] Y. Wang, Y. Sui, J.G. Cheng, X.J. Wang, W.H. Su, J. Phys. D: Appl. Phys. 41 (2008) 045406.
[17] C.J. Liu, L.C. Huang, J.S. Wang, Appl. Phys. Lett. 89 (2006) 204102.
[18] D. Li, X.Y. Qin, Y.J. Gu, J. Zhang, J. Appl. Phys. 99 (2006) 053709.
[19] B.C. Zhao, Y.P. Sun, W.J. Lu, X.B. Zhu, W.H. Song, Phys. Rev. B 74 (2006) 144417.
[20] Y. Wang, Y. Sui, J.G. Cheng, X.J. Wang, W.H. Su, X.Y. Liu, H.J. Fan, J. Phys. Chem. C 114 (2010) 5174.
[21] Y. Wang, Y. Sui, P. Ren, L. Wang, X.J. Wang, W.H. Su, H.J. Fan, Chem. Mater. 22 (2010) 1155.
[22] G.D. Tang, C.P. Tang, X.N. Xu, Y. He, L. Qiu, L.Y. Lv, Z.H. Wang, Y.W. Du, Solid State Commun. 150 (2010) 1706.
[23] R. Asahi, J. Sugiyama, T. Tani, Phys. Rev. B 66 (2002) 155103.
[24] Y. Wang, L.X. Xu, Y. Sui, X.J. Wang, J.G. Cheng, W.H. Su, Appl. Phys. Lett. 97 (2010) 062114.
[25] R.D. Shannon, Acta Crystallogr. Sect. A 32 (1976) 751.
[26] B.C. Zhao, Y.P. Sun, W.J. Lu, J. Yang, X.B. Zhu, W.H. Song, Solid State Commun. 139 (2006) 209.
[27] J. Lan, Y. Lin, G. Li, S. Xu, Y. Liu, C. Nan, S. Zhao, Appl. Phys. Lett. 96 (2010) 192104.
[28] Y.N. Huang, B.C. Zhao, Y.P. Sun, X.B. Zhu, J.M. Dai, (manuscript prepared).
[29] P. Limelette, V. Hardy, P. Auban-Senzier, D. Jerome, D. Flahaut, S. Hebert, R. Fresard, C. Simon, J. Noudem, A. Maignan, Phys. Rev. B 71 (2005) 233108.